ARIES-AT Magnet Systems

F. Dahlgren, T. Brown, P. Heitzenroeder
Princeton Plasma Physics Laboratory, Princeton, NJ 08543

L. Bromberg,
M.I.T. Plasma Science & Fusion Center, Cambridge, Ma, 02139-4307

and the ARIES Team

This report presents a conceptual design of the magnet systems for an advanced tokamak fusion reactor (ARIES-AT). The main focus of the paper is to anticpate and extrapolate the current state-of-the-art in high temperature superconductors and coil design, and apply them to an advanced commercial fusion reactor concept. The current design point is described and supported with a preliminary structural analysis and a discussion of the merits, performance, and economics of high temperature vs. low temperature superconductors in an advanced fusion reactor design.

Key Words: Fusion, magnet, superconductivity, ARIES, HTS, YBCO

I. INTRODUCTION

The ARIES-AT reactor is a conceptual commercial reactor based on aggressive extrapolation from the present engineering database, with modest extrapolation in the physics database. In contrast with ARIES-RS[1], both the physics and the engineering are more aggressive.

The design of the toroidal field magnet is slightly less demanding than the ARIES-RS due to improved physics. As with the ARIES-RS Magnet[2], the magnet is steady state, with limited numbers of transients. The magnet issues for ARIES-AT are different from previous ARIES designs, in that they are manufactured using high temperature superconductors (HTS).

HTS have been shown to have high current densities at high fields, and therefore magnets can be designed for high field operation, limited by structural issues. In the system code analysis, the use of high magnetic field option was allowed. However, it was found that the system optimized (in terms of cost of electricity) at moderate magnetic fields that are achievable with conventional low temperature superconductors. The peak field in ARIES-AT is 11.1T at the TF coil and 9T at the PF coils.

The use of high-Tc (Tc – critical temperature) has important implications on the critical issues of the toroidal and the poloidal field systems[3]. The objective of the magnet work in ARIES-AT is to review options for unconventional magnet design with HTS. In particular, the reference ARIES-AT design uses a HTS that is continuously graded, with epitaxial manufacturing methods for the conductor.

This paper provides the background utilized by the systems code to evaluate the options. The paper also provides detailed engineering calculations of the critical issues. Improvements on the magnet design and construction that could result in decreased cost of the toroidal and poloidal field magnets have also been investigated. The extrapolated cost of HTS-based magnets is analyzed. Improved manufacturing techniques for the magnets are illustrated. Incorporating these techniques and improved design concepts into TF and PF magnets suitable for a commercial tokamak reactor remains a difficult challenge.

The superconductor and structural materials, are briefly discussed in Sec. II. Sec. III discusses some HTS issues and magnet cooling options. Sec. IV provides details on the design of the reference ARIES-AT TF coils. The finite-element structural analysis is presented in Sec. V The engineering details of the PF system for ARIES-AT are described in Sec.VI. The cost assumptions of the TF and PF systems are described in Sec. VII

II. MATERIAL OPTIONS:

The reference case of ARIES-AT is a moderate field tokamak with HTS superconductors. The HTS materials are not available presently, and therefore assumptions must be made as to what may be available in the future. In this section the material properties of the materials for the design of the ARIES-AT magnets are presented.

a. Superconductor options

Figure 1. shows the critical current density as a function of temperature for several HTS and LTS materials. At temperatures greater than about 20K, the only HTS material that looks promising for fusion applications from those shown in the figure is YBCO tapes. BSSCO has great performance particularly at high fields, although at low temperatures[4].

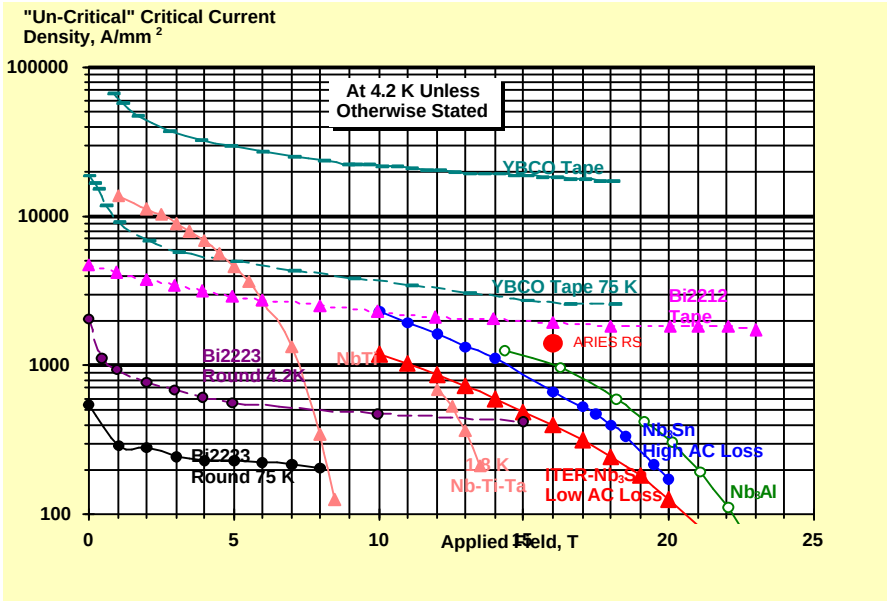

Figure 1. Critical current density for several HTS and LTS materials as a function of the applied field, for either liquid nitrogen temperature or 4 K (if not indicated).

The performance of YBCO at liquid nitrogen temperature and 10 T is comparable to that of non-copper current density of Nb_3Sn superconductor, at 4 K and 0 T. Indeed, once the structure and stabilizer/quench protection is included in the Nb_3Sn designs, the average current density in the Nb_3Sn conductor is substantially lower than that for YBCO at elevated temperatures.

For YBCO thick film conductors, the superconductor is not single crystal but single domain. The c-axis is perpendicular to the tape. The superconducting YBCO film is highly textured with the ab plane parallel to the surface of the tape. A large amount of anisotropy exists in the superconductor, depending whether the magnetic field is aligned with the c-axis or perpendicular to it. The difference is especially large at the higher temperatures. The tapes can support limited values of field aligned to the c-axis.This is shown for YBCO in Figure 2[4].

The actual performance of the superconductor is a strong function of the HTS film thickness. Presently, the thinner the film the higher the current density. It has been assumed in this study that eventually it would be possible to make relatively thick films (on the order to 20 – 30microns) of long lengths, with properties comparable or better than those shown in Figures 1 and 2.

In order to minimize the expense, it has been assumed that the conductor can be manufactured by epitaxially depositing the HTS material directly on the structure, with intermediate layers if necessary. The scheme is illustrated in Figure 3. For the TF coil, the structural material is in the form of a continuous shell that is wound after the material has been heat-treated. For the poloidal field coil, the HTS is deposited on flat pancakes that are then assembled into a coil.

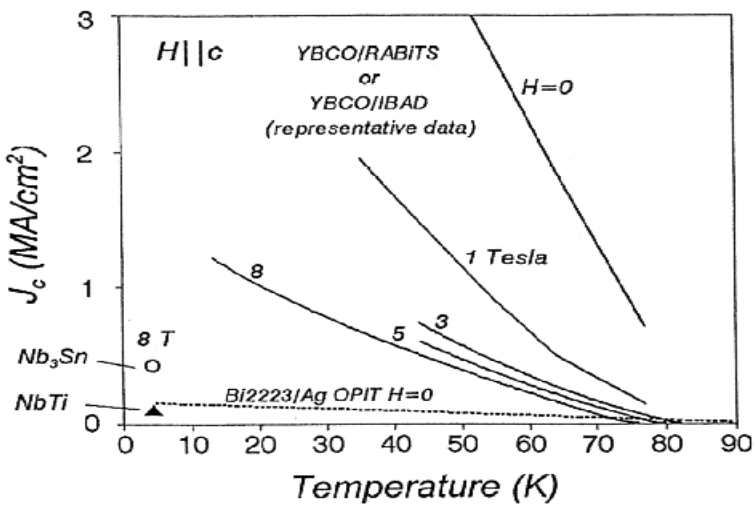

Figure 2. YBCO current density for fields perpendicular to the tape.

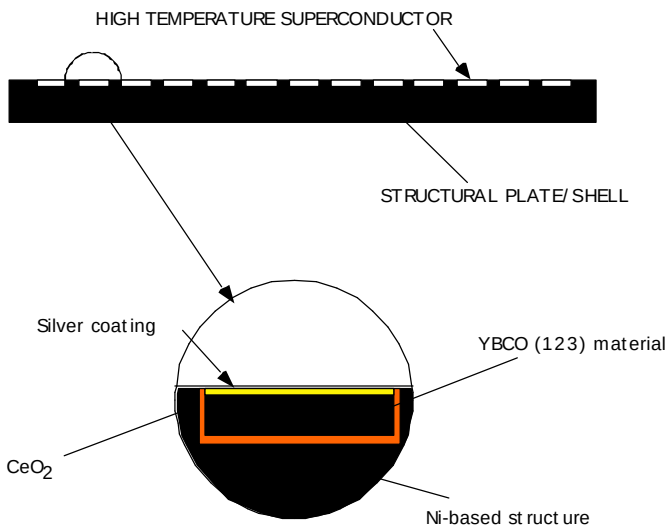

Figure 3. Magnet construction using epitaxially deposited YBCO thick films.

III. HTS CONDUCTOR DISSCUSSION:

a. Stabilizer and quench protection in HTS magnets for fusion

High temperature superconductors do not suffer from flux-jumping when operated at temperatures higher than about 10-20 K, because of the very high thermal capacity of the metals at these temperatures (about 2 orders of magnitude higher than at 4K). As a result, there is no need for a substantial fraction of normal conducting material, in contrast with LTS materials. A very large source of energy is required to start a quench. The only normal conducting material required is whatever is needed to manufacture the superconductor. In the case of YBCO, it is a Ni tape. For BSCCO, the filaments are likely to be placed in a silver matrix.

The high thermal capacity of high Tc materials increases the difficulty of quench-detection, mainly because the quench-zone propagates very slowly in high-Tc superconductors[5]. Figure 4. shows characteristic times for propagation of a quench in low temperature and high temperature superconducting wires. The results for BSSCO 2212 wires indicate at least one order of magnitude decrease in the speed of quench propagation, making it very difficult to detect a quench in a large coil. For active magnet protection, novel methods of quench protection and quench detection are required if the applications of high-Tc superconductors at high temperatures is to become a reality.

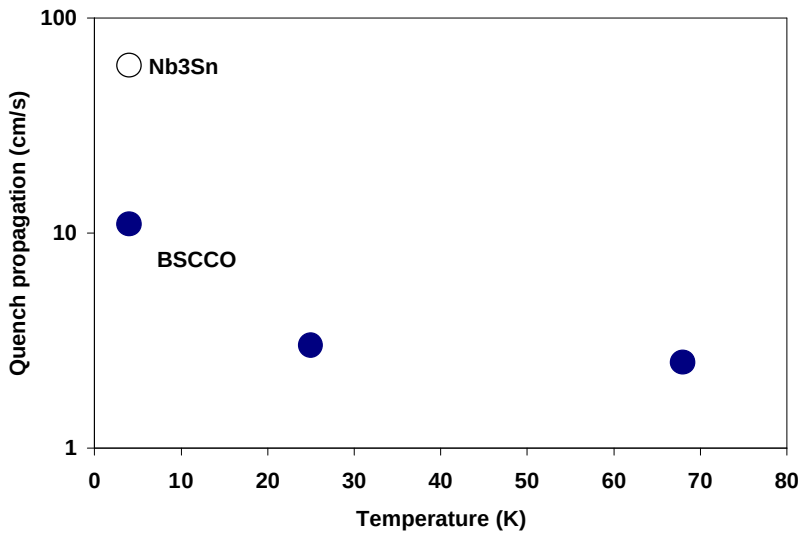

Figure 4. Quench propagation speed in LTS and HTS (2212 BSSCO).

For ARIES AT, it is assumed that all of the stabilizer and quench protection normal conductor could be eliminated from the coil.

In conventional low temperature superconducting magnets, quench protection dominates the conductor cross section. Since the cost of the conductor is a substantial fraction of the total cost of the coil, the cost of the quench protection could be a substantial driver in the coil cost. With decreased superconductor (due to high current densities), stabilizer and coolant, the structural fraction of the cross section can be increased substantially. The elimination of the

stabilizer, and the need to have the coolant in close proximity to the superconductor, may allow for simple epitaxial manufacturing techniques that should decrease the cost of manufacturing the magnet.

b. Radiation limits

1. Superconductor

At the present time, the threshold fluences for damage of the superconductors have not been determined. Published data in the high fluence regime are scarce. Kuepfer quotes Tc's for a flux of 10^{23} neutrons/m^2 (E>1 MeV). Sauerzopf [7] gives results for fluxes of up to $1.2x10^{22}$ neutrons/m^2. His group also has two data points at a higher dose[8]. The highest neutron fluence to-date was $2.8x10^{22}$ neutrons/m^2 and Tc was 81 K. Both results were obtained without annealing.

For Nb_3Sn, the neutron fluence beyond which critical current degrades is about $3x10^{22}$ neutrons/m^2. The irradiation resistance of YBCO is at least as good as, and could be better than that of Nb_3Sn.

2. Insulation

Organic as well as inorganic materials are under consideration for use as insulation material. Most superconducting magnets are presently manufactured using fiber-reinforced epoxy, which imposes a relatively low limit on the allowable irradiation.

The radiation limit for organic insulators is on the order of 10^8 rads for fiber-reinforced epoxy and 10^9 rads for polyimide based insulation. These limits are for the case when the insulator needs to withstand substantial shearing forces. In the absence of shear, it is possible to increase these limits, by as much as a factor of 10.

The fluence limit for inorganic insulators is determined by swelling. For practical insulators the maximum irradiation ranges from 10^{11} rads to 10^{14} rads depending whether the insulator is in sheets or in powder form. The corresponding neutron fluence (>0.1 MeV neutrons) is 10^{24}-10^{27} neutrons/m^2.

In the case of YBCO, an insulator is used in the manufacturing process, as a compliant buffer layer between the thick YBCO films and the Ni substrate. There may be no need for an organic-based insulator. It may be assumed that the irradiation limit of the insulators for HTS magnets can be increased to 10^{11} to 10^{14} rads, depending on whether or not the insulator experiences shear loads.

When compared to LTS materials, HTS materials have the potential of substantially relaxing the design restrictions placed on the material by irradiation damage to insulation, the stabilizer and nuclear and AC heating of the cryogenic environment. However, the information available today only indicates that irradiation damage limits of HTS material itself is not lower than for the LTS materials.

c. Coolant choice and cooling geometry

Because of the limited temperature of operation of materials other than YBCO, the choice of coolant is limited to either high pressure helium gas, or liquid nitrogen. Helium gas and neon are the only practical coolants between 4K and liquid nitrogen temperature. The interest in simplifying the design and decreasing the cost drove the design to a liquid nitrogen system, eliminating all but YBCO as the superconductor.

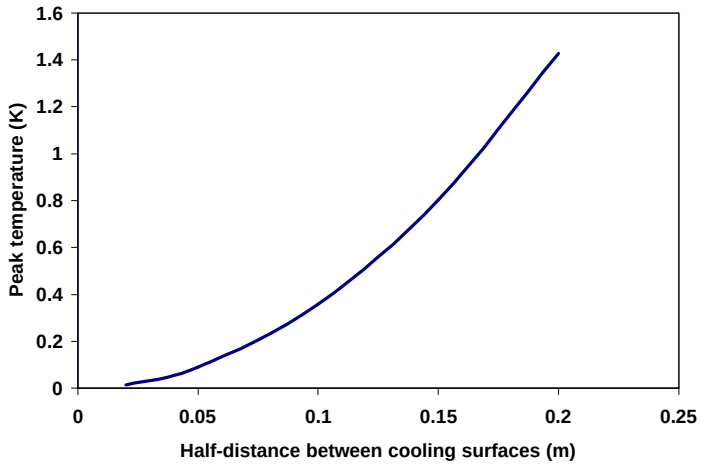

Figure 5. Temperature rise for a steel plate with 500 W/m^3 of nuclear heating, as a function of the plate half-width.

Because of the high temperature and because of the large thermal capacities and temperature margins, it is possible to remove the coolant from being in direct contact with the conductor, and instead cool the edge of the plates (TF) or the edge of the pancakes (PF). The worst condition occurs at the TF, because it is there that the nuclear heating peaks. In order to determine the effect of edge cooling of the plates, the temperature drop across the plate was calculated, for different plate widths, using a 1.5-D compressible thermal analysis of the coil[5]. The results are shown in Figure 5. where it is assumed that the nuclear heating is 500 W/m^3. It is found that the temperature raise at the centerline of the plate, assuming cooling at both edges of a steel plate, is on the order of 1 K.

In addition, in order to increase the performance of the superconductor and to allow for increased temperature margins, subcooled liquid nitrogen was used. Thus it was possible to cool the entire plate without going into the film boiling. Figure 6. shows the temperature along the coolant channel, for an inlet nitrogen temperature of 68K. The length of the innermost shell in the toroidal field coil is on the order of 36 m. Shown in the figure at the average magnet temperature and the average coolant temperature. It was assumed that the velocity of the liquid nitrogen was 3 cm/s, with a pressure drop of about 0.3 MPa. Higher velocities would result in substantially decreased temperature rise in the coolant, if it is desired or needed to keep the temperature of the outlet lower than indicated in the Figure.

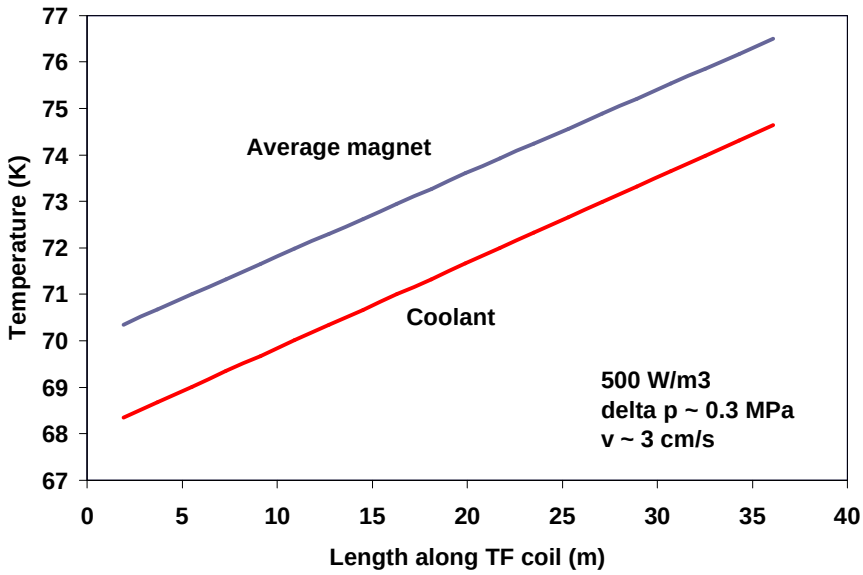

Figure 6. Average magnet and coolant temperature along the cooling channel, with subcooled liquid nitrogen. One channel at each edge of the shell used to wind the TF coil.

d. Summary

For the ARIES-AT study, YBCO tapes were chosen as the conductor, because of its ability to operate at much higher current density at liquid nitrogen temperatures. YBCO tape operating at liquid nitrogen temperatures tolerates moderate (~5 T) magnetic fields that are perpendicular to the tape. The coolant is subcooled liquid nitrogen, flowing along the edges of the plates, with a length of one turn for the case of the toroidal field. At the present time, it has been demonstrated that the radiation limit of the HTS is no lower than for the LTS, allowing for the use of advanced organic insulators. Inorganic insulators are used in each turn in the coils, since they are an integral part of the manufacturing process of the superconductor. For ground wrap insulation, materials similar to those used in LTS are used.

IV. MAGNET SYSTEM DESIGN:

The Aries-AT toroidal field (TF) and poloidal field (PF) configuration has been designed to permit full replacement of the blanket/shield modules located within the vacuum vessel (VV). Access for these modules are provided by developing a TF design that places no structure in the horizontal port region, allowing the vacuum vessel port to extent unrestricted radially outward. Figure 7. shows the overall general arrangement of the Aries-AT device highlighting the TF system and PF ring coils that are mounted to the TF structure.

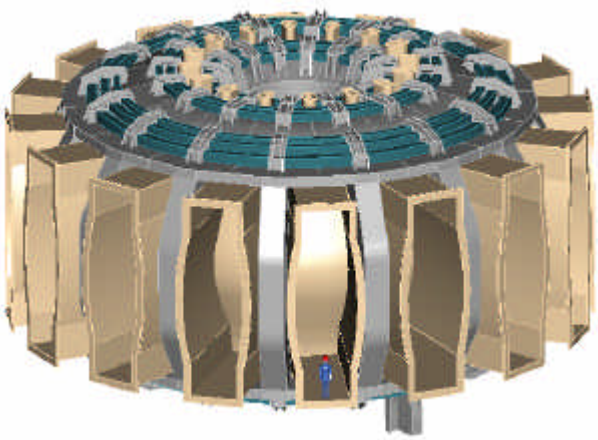

Figure 7. Aries-AT General Arrangement

The TF design consists of 16 wedged TF coils that operate at 75° K using YBCO high temperature superconductor on an Inconel strip. The coils develop a 5.9 T field at the plasma major radius of 5.2 m. The TF support system, coil shape and superconductor-winding scheme were developed to match an earlier defined vacuum vessel shape. Figure 8.0 shows a sector module to illustrate the interface between the TF, vacuum vessel and in-vessel components. The TF structure was shaped and placed in a close proximity to the vacuum vessel while allowing space for a thermal shield and gaps for differential movement between the TF and vacuum vessel. Figure 9. illustrates configuration details of a TF/VV sector highlighting section views and local details. To extract a full shield module required the shape of the VV horizontal ports to be vertically extended with sharp corners that restricted the ability of placing supporting structure to help support the overturning forces acting on the TF coil (see Section E-E of Figure 9.). Also the shape of the vacuum vessel in the upper

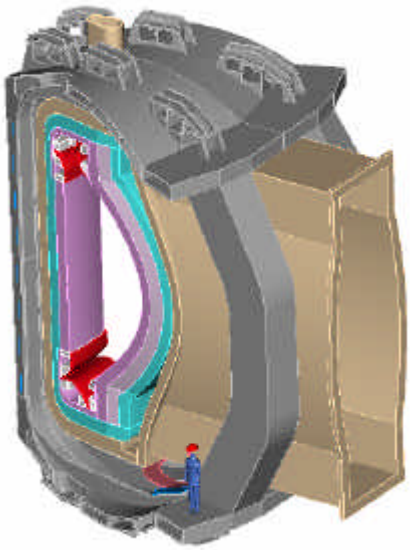

Figure 8. TF/VV sector

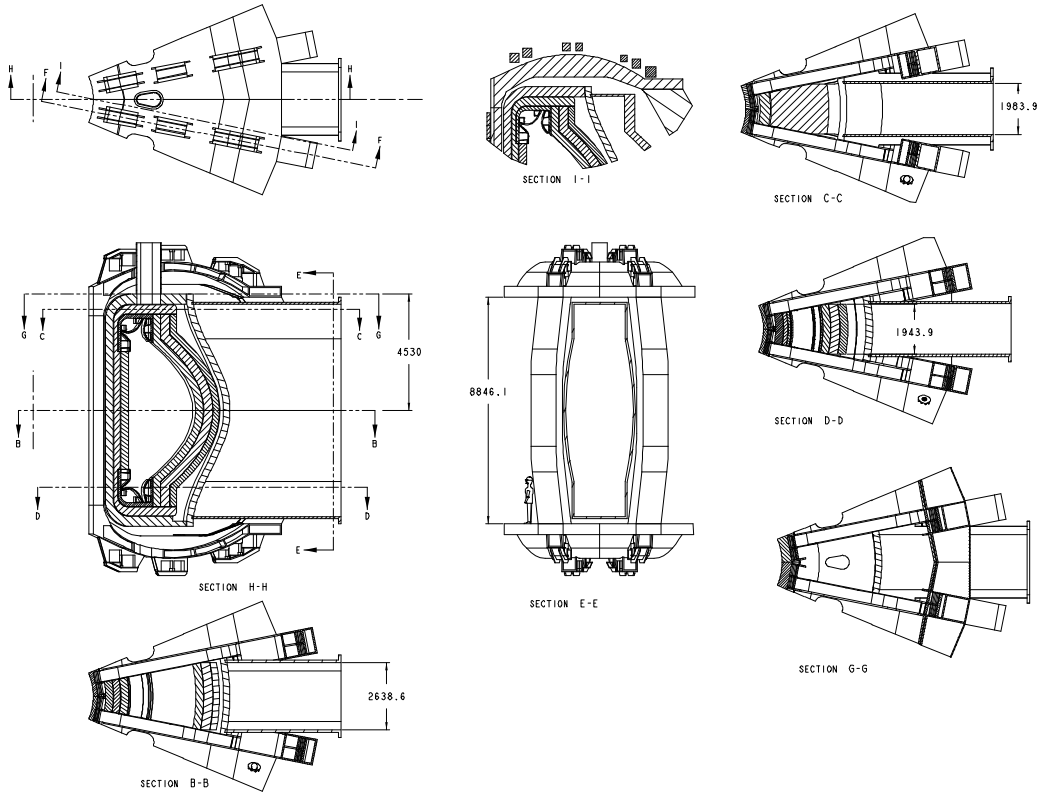

Figure 9. TF/VV Sector Geometry Details

and lower inboard region near the divertors (see Section H-H) placed restrictions on locating TF coil structure in the corner regions that could improve the design in supporting the overturning forces acting on the TF inner leg. Future iterations in refining the shapes of the divertor, shield and vacuum vessel in this local region would allow for a more efficient TF structure.

The structural details of the TF case are shown in the isometric cut-away view of Figure 10. The double pancake, high temperature superconductor is nested in the case with a center rib separating the pancake windings. A 10 cm inner case structure is added on the plasma side to increase the torsional stiffness of the structure. Wedging between adjacent coils supports the centering force acting on the inner leg. To increase the out-of-plane stiffness of the outboard leg, the case structure was built up in the radial direction as shown in Figure 10. The intercoil structure is a double wall ribbed structure that conforms to the contour of the vacuum vessel and forms a flat region above/below the horizontal ports. Local stiffening ribs have been added in the curved region of the structure to increase its overall stiffness. Figure 11. shows a full isometric view of a

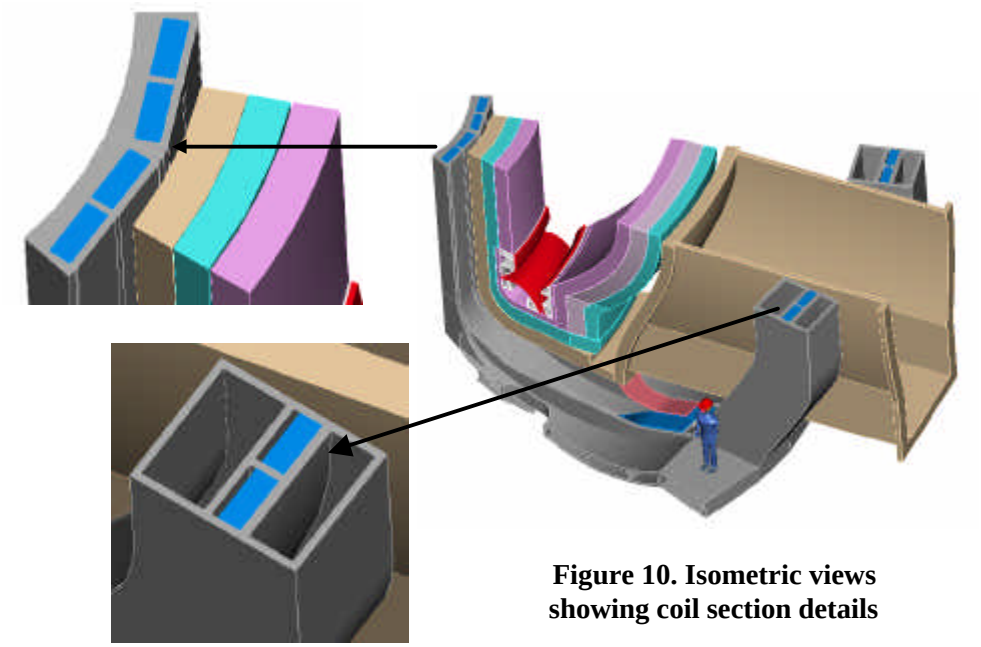

Figure 10. Isometric views showing coil section details

single TF coil which includes the power lead support details. One of the sixteen coils has the lead support structure while the remaining fifteen coils are configured for coil-to-coil lead connections. Further details of the leads and their support scheme can be seen in the isometric views of Figure 12. The full assembly of the all sixteen TF coils is shown in this figure. One coil provides the structure to support the input and exit leads and "U" shaped jumpers forms the coil-to-coil connections. The structural support details required for the jumpers have not been developed. With the full assembly of the TF coil system the vacuum vessel and in-vessel components can be assembled through the large access area between the TF outer legs.

Figures 9. through 12. also show the PF ring coil support structure. Local ribs with cover plates have been added to the upper and lower intercoil shell structure that will be used to locate and react the vertical loads acting on the PF coils.

To minimize the overall cost of the TF case a large portion of the coil structure would be fabricated as castings. Rolled plates would be used in those areas of high stress where higher material properties are warranted. Figure 13. shows an exploded view of the coil case major sub-assemblies. The total weight of a single TF coil is 64 metric tons. The double pancake conductor (shown in Figure 13.) is wound into

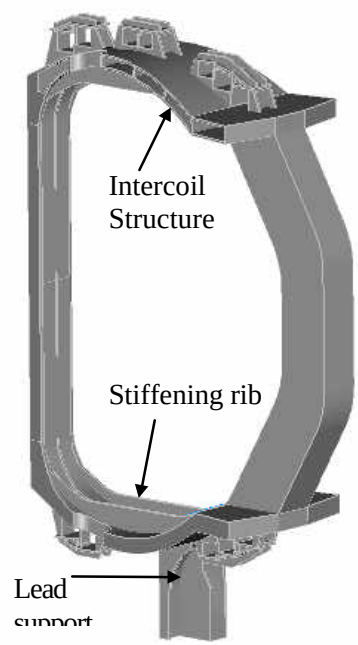

Figure 11. TF coil

the coil case channel from two spools that are sized to limit the conductor strain to a value less than 0.2% strain.

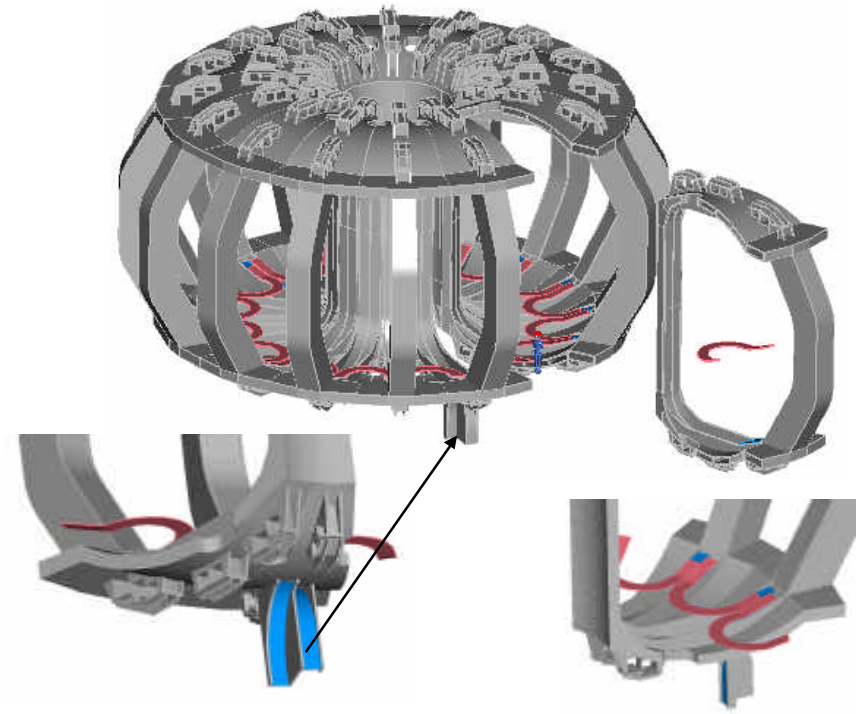

Figure 12. Full TF coil assembly and local lead details

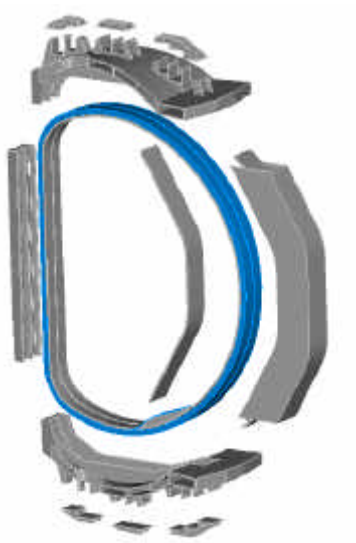

Case exploded view

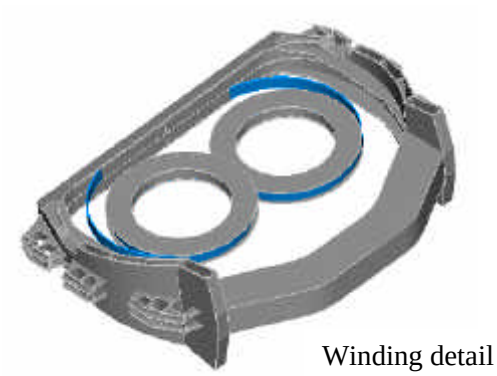

Winding detail

Figure 13. TF coil exploded view and coil winding detail.

V. COIL AND STRUCTURAL ANALYSIS:

FEA Model Description:

The TF coil is modeled with MSC/Nastran[9] using standard hexahedral solid brick elements and triangular and quadrilateral plate elements (see Figure13.). A reduced modulus was used to represent the average effective properties of the conductor/substrate composite. Plate elements were used to model the inter-coil structure. The boundary conditions were modeled using multi-point and single point constraints. Single point constraints were applied to selected points of symmetry to eliminate the rigid body displacement modes, while multi-point constraints were used to model the coil to coil interface (see the TF Coil Loads and Load Paths discussion below). The two heavy ring structures at the outboard top and bottom of the coil outer leg were modeled using solid elements and together with the outer leg, provide much of torsional stiffness to the structure. The preliminary model developed did not have any additional vertical structure at the inner coil leg bore and used 2" thick case walls in the outer vertical leg section. The large vertical gap between the upper and lower rings presents some significant difficulties in designing a torsionally stiff coil structure. (This is a design constraint imposed by the clearance required for radial extraction of the blanket module). It was found that excessive torsional displacements resulted. Subsequent model runs included an additional vertical ligament at the inner coil bore and a substantially increased wall thickness and inter-coil structure to resist the out of plane bending of the coil. No attempts were made in this analysis to model the residual stresses or winding stresses in the conductor or substrate. The minor thermal effects due to cool down were also not included.

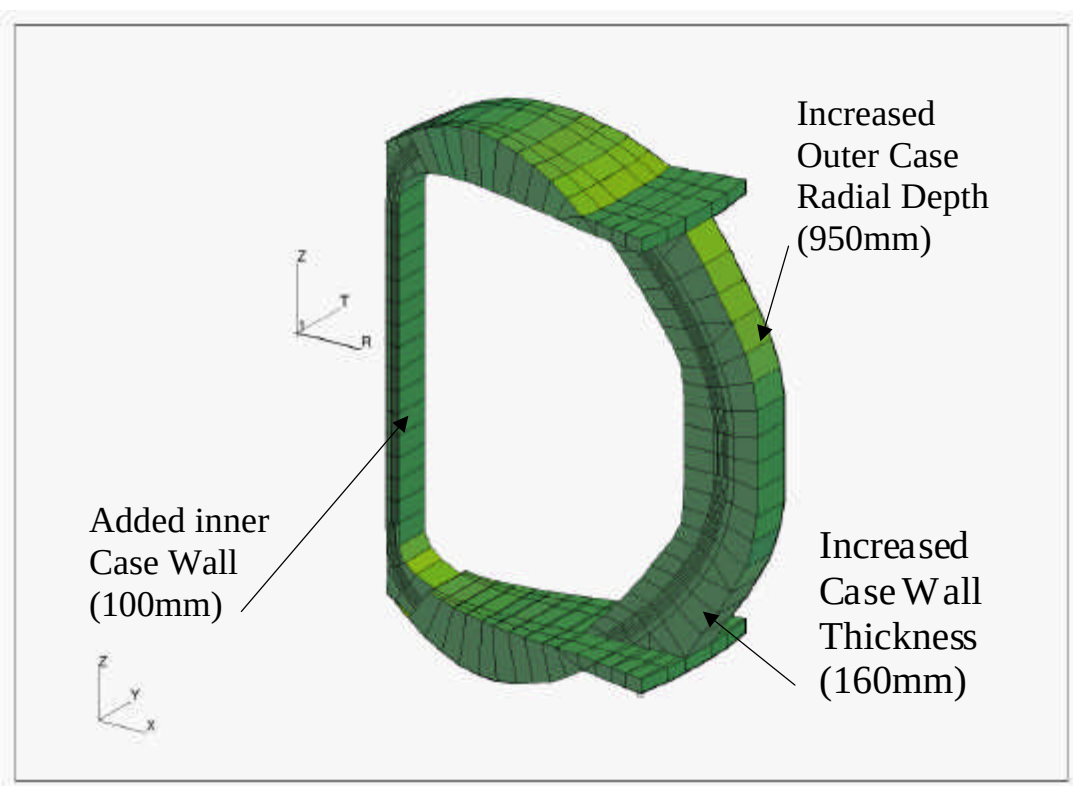

Figure 13. Aries-AT TF Coil/Case FEA Model With Reinforced Walls

TF Coil Loads and Load Paths:

The primary loads on the coils and coil support structure are the result of the Lorentz forces acting on the conductor due to the interaction of self fields perpendicular to the current or external fields produced by the other coil systems. In particular, the in-plane loads on the TF Coil are almost exclusively due to self fields. These in-plane loads peak at the inner coil leg and diminish inversely with the radius (due to the 1/R toroidal field component). The largest out of plane loads on the TF Coils are primarily due to magnetic fields normal to the TF Coil current produced by the Poloidal Field Coils which are in close proximity to the TF conductors. These out-of-plane forces and a map of the field contours that produce them are shown in Figures 14a. & 14b.

Figure 14a. Out of Plane loading

Figure 14b. Polloidal Field Contours On TF Coil

For the out-of-plane forces the load path generally is from the HTSC to the substrate and ultimately into the coil case and external support structure. It is primarily the overall bending stiffness of the coil case and top to bottom stiffness of the complete structure that determines the out of plane flexure of the coil. Since this is a wedged coil design a significant aspect of the overall out-of-plane behavior of the coil/case structure is the friction force which develop between adjacent coil case wedge faces at the inner coil legs. These friction forces act to inhibit the relative radial and vertical motion of adjacent coil surfaces and tend to allow the inner coil case to act more or less as a torsionally rigid cylinder rather than as individual vertical ligaments. This torsional stiffening in turn helps resist the out of plane flexure of the inner coil leg. To properly model this effect it is usually necessary to use non-linear elements in the FEA model that have a stiffness that is a function of the friction coefficient and the normal local (wedging) loads being applied. This is particularly important in the upper and lower corners of the TF coil where the net radially outboard forces (developed in the outer leg of the TF coil) tend to unload the wedging forces and reduce (or even eliminate) this friction force. Nastran has non-linear gap elements

which would normally be used to model this boundary condition, however due to the limited scope and budget available for the project, it was decided to forgo the expensive and time consuming non-linear analysis and use MPCs (Multi-Point Constraints) to model wedge surface interfaces. This has the effect of artificially locking the adjacent coil case wedge surfaces together and implicitly assumes that the friction forces developed on the wedge surface are sufficient to balance the shear forces existing between coils due to the out of plane loads. To more accurately reflect the reduced friction at the upper and lower corners, two iterations of the static analysis were performed with the MPCs being removed in areas were the wedge forces were positive (ie. Where un-wedging occurred). While this approach still tends to somewhat overestimate the torsional stiffness of the inner coil/case leg, it was confirmed there is sufficient space and material in the side walls to provide some form of shear-key or vertical and radial interlocking mechanisms to supplement the friction forces in this design should this be necessary. Were we to pursue the development of this design beyond it's current level implementing interlocking wedge surfaces and radially preloaded support rings at the upper and lower corners of the TF coil bore would be two possible means to help stiffen the structure and provide a reaction to radial outboard loading from the outer leg.

The loads from the in-plane forces are generally shared by the conductor substrate and the coil case in parallel. Since the substrate and case comprise 85% of the total cross sectional area of the TF Coils/case, the majority of the in-plane loads will be carried by the case and substrate.

Results and Discussion:

As mentioned above the initial coil/case structure was not adequate to resist the out of plane TF loads, so a 100mm thickness was added to the inner case wall and the outer leg coil case wall was increased from 50mm to 160mm along with an increase in the radial depth to 950mm as indicated in Figure 13. A less rigid case would not perform adequately with the requirements of the HTSC. The use of HTSC establishes certain constraints on the TF coil design and case structure. Specifically the need to limit the total strain in the conductor material to less than 0.2%. The main area of the coil where this presents a significant problem is at the upper and lower inner corners of the TF coil due to the flexing of the coil structure in response to the in-plane and out-of-plane loads. Figure 15. shows the peak out of plane deflection of the coil of the preliminary coil/case structure of 130mm prior to stiffening the outer leg and ring sections. This preliminary coil/case configuration was not stiff enough to prevent large strains in the HTSC conductor in the problem areas as shown in Figure 16. The maximum strain can be seen to be > 7.5%.

Figure 15. Out of Plane Displacements (mm) In the Preliminary TF Coil/Case Model

Figure 16. Strains In the Preliminary TF Coil/Case Model Due to Out Of Plane Loads

A stiffer outer case leg and adding a vertical structural ligament to the inner bore of the coil model greatly mitigated this condition however further stiffening of the case and rings will probably be desirable to bring the strain below the 0.2% limit. Since these results do not include the residual compressive strain due to cool down they represent an upper bound on the tensile strain in this region. The compressive strain locked-in from the reaction

temperature on down to 77 ^{o}K should relieve this somewhat. Figure 17. indicates that the corner strains are 0.37% with the improved coil/case design.

Figure 17. Out of Plane Displacements – Reinforced Case Model

Figure 18. Reduced Strains With a Stiffened Coil Case Structure

Figure 19 . Peak Tresca Stress in the Reinforced Coil Case

Figure 19. shows the Tresca stress contours in the coil case peaking at about 480 MPa with maximum primary stresses in the 300 MPa range which should provide adequate margins over the design allowables for most Inconel alloys. As a typical example Inconel 625 has a yield strength of over 900 MPa at 77 ^{o}K and an ultimate strength of over 1200 MPa. Assuming a 1/3rd S_{ult} and 2/3rd S_{yp} criteria, maximum primary stresses allowed would be 408 MPa.

VI. Poloidal Field Coils:

Table I and Figure 20. below is a summary of an optimized poloidal coil configuration and the total currents for a typical discharge. Table II shows the maximum stresses for the typical currents indicated with a 12.95 MA plasma current and with no Plasma current present. The maximum stress is 442 MPa in coil #14 with the Plasma current present. The majority of this stress is the tangential stress with the primary hoop component being 424 MPa, and will be reduced by increasing the coil cross section. This increase in cross section is also necessary to reduce the current density in this coil. All PF coils are self supported in the radial direction. With the cross section composed of 85% structure and substrate, the maximum strain in the PF coils is less than the 0.2% prescribed allowable strain limit for the HTSC material. The present analysis reflects 54 kA/sq.mm for the PF Coil current density.

Figures 22. & 23. shows a detailed field map in the area of the various PF coil cross sections. A potential problem arises when the peak fields perpendicular to the current plane exceed 5.8 Tesla (assuming the 54kA/sq.mm current density). The reason for this can be seen by examining the graph of critical current vs. fields shown in Figure 21. From this plot it can be seen that the critical current is far more sensitive to fields oriented perpendicular to

the current plane than fields parallel to it. Figure 23. indicates that PF-14 will exceed the critical current for the ambient fields at the conductor. A reorientation of the HTSC conductor plane and a reduction in current density is needed to address this condition. Figure 24. shows a peak vertical field at the HTSC of 7.5 T for a 30 kA/mm^2 current density with a horizontally re-oriented conductor winding. Alternatively as discussed above, the temperature of the superconductor could be decreased to about 68K, facilitated by the use of the liquid nitrogen coolant temperatures between boiling and freezing, and due to the very small nuclear heating of the PF coils.

	8	3.25	5.750	6.348
	9	3.75	6.000	6.518
Ring	10	5.25	6.300	4.810
Coils	11	5.75	6.250	3.643
	12	7.50	5.650	-3.276
	13	8.00	5.400	-5.877
	14	8.50	5.100	-8.624
	Coil	**R**	**Z**	**I**
	Number	**(m)**	**(m)**	**(MA)**
	1	2.25	0.250	-0.620
	2	2.25	0.750	-1.053
	3	2.25	1.250	-1.513
OH	4	2.25	1.750	-1.523
	5	2.25	2.250	-0.665
	6	2.25	2.750	1.184
	7	2.25	3.250	3.360

Table I. Optimized PF Coil Set Locations and Currents

		Ip=0		Ip=12.949 MA	
Coil	A-t	ksi	Mpa	ksi	Mpa
1	-0.65	4.94	34.18	1.52	10.5184
2	-1.05	7.98	55.22	2.27	15.7084
3	-1.55	10.087	69.8	3.27	22.6284
4	-1.52	9.002	62.29	4.35	30.102
5	-6.65	2.306	15.96	3.035	21.0022
6	1.18	0.1455	1.007	8.363	57.872
7	3.36	9.659	66.84	30.86	213.551
8	6.518	38.52	266.6	43.35	299.982
9	4.81	17.25	119.4	10.73	74.2516
10	3.643	10.49	72.59	7.147	49.4572
11	-3	39.81	275.5	37.95	262.614
12	276	40.5	280.3	39.88	275.97
13	-5.88	49.05	339.4	48.32	334.374
14	-8.62	59.65	412.8	63.98	442.742

Table II. PF Coil Currents and Peak Stresses For Optimized Coil Set

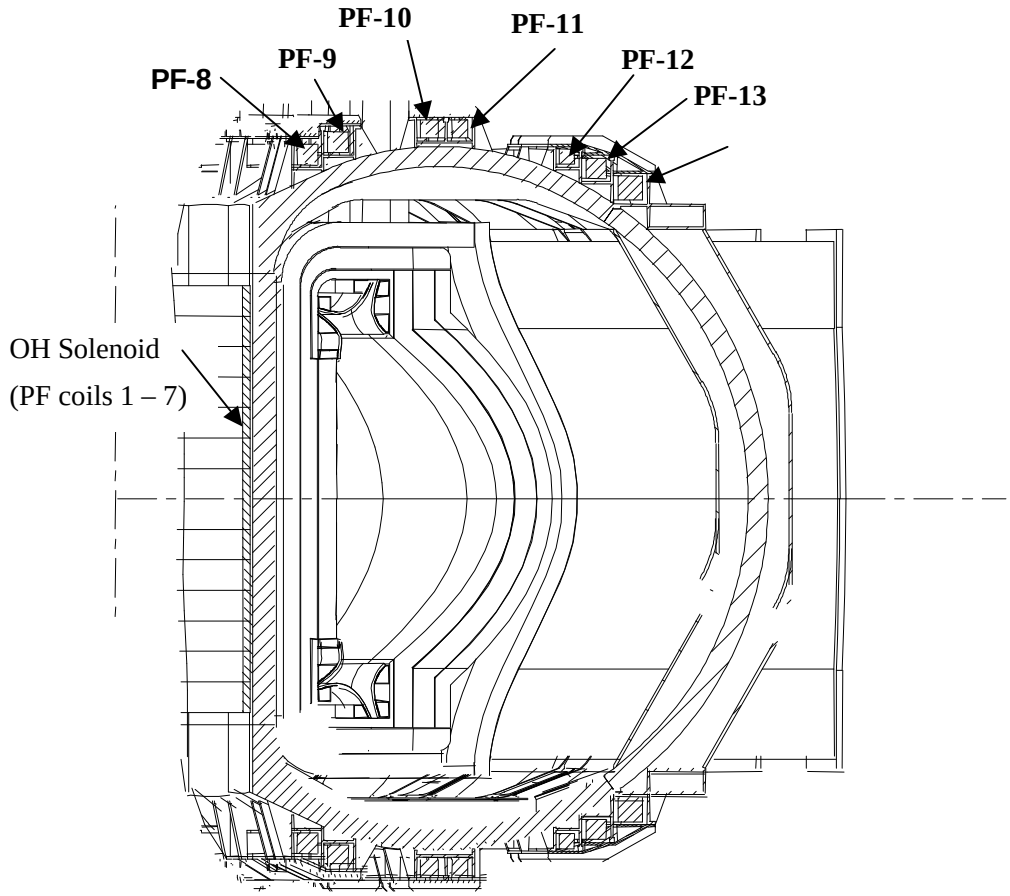

Figure 20. PF Coil Locations

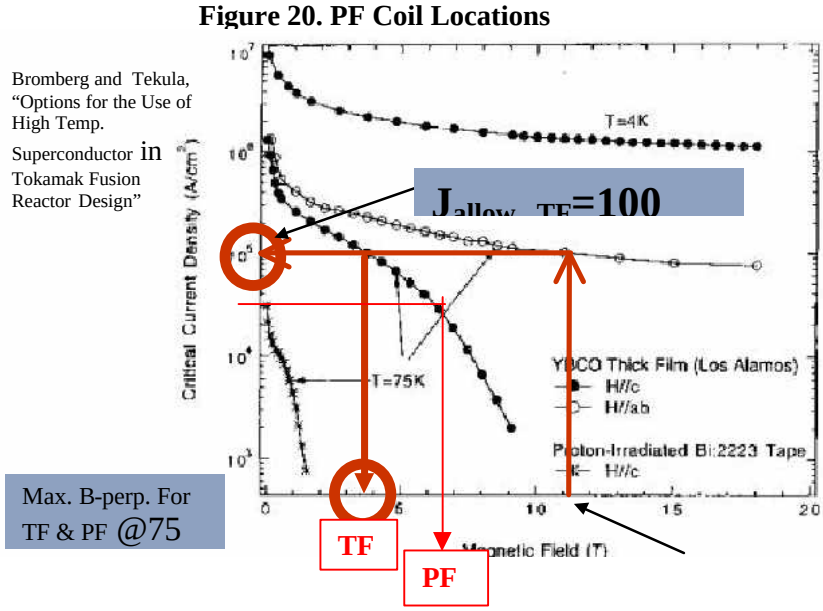

Figure 21. Critical Current Density for YBCO-123 as a Function of Field

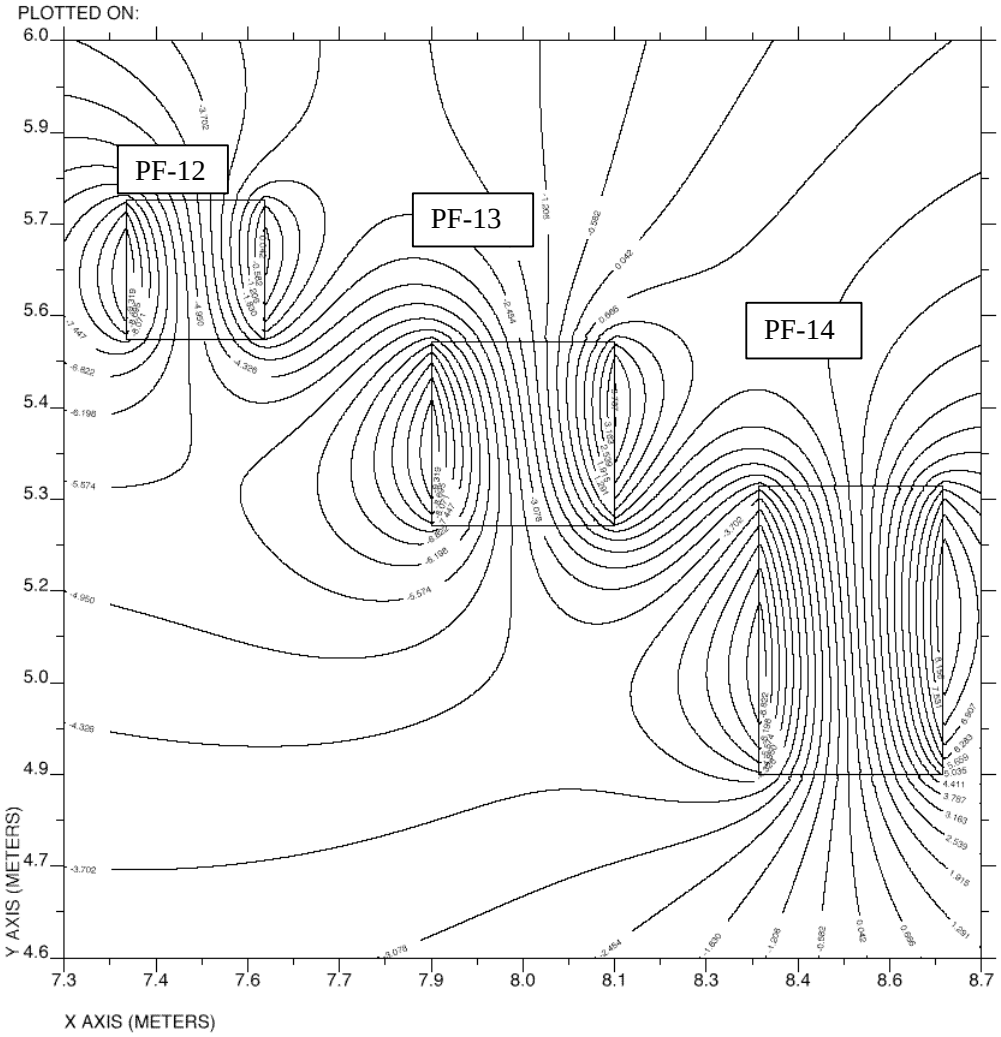

VERTICAL FIELD CONTOUR PLOT ARIES-AT PF COIL OPTIMIZED-L

Figure 22. Vertical Field Contours At PF-12, PF-13, & PF-14

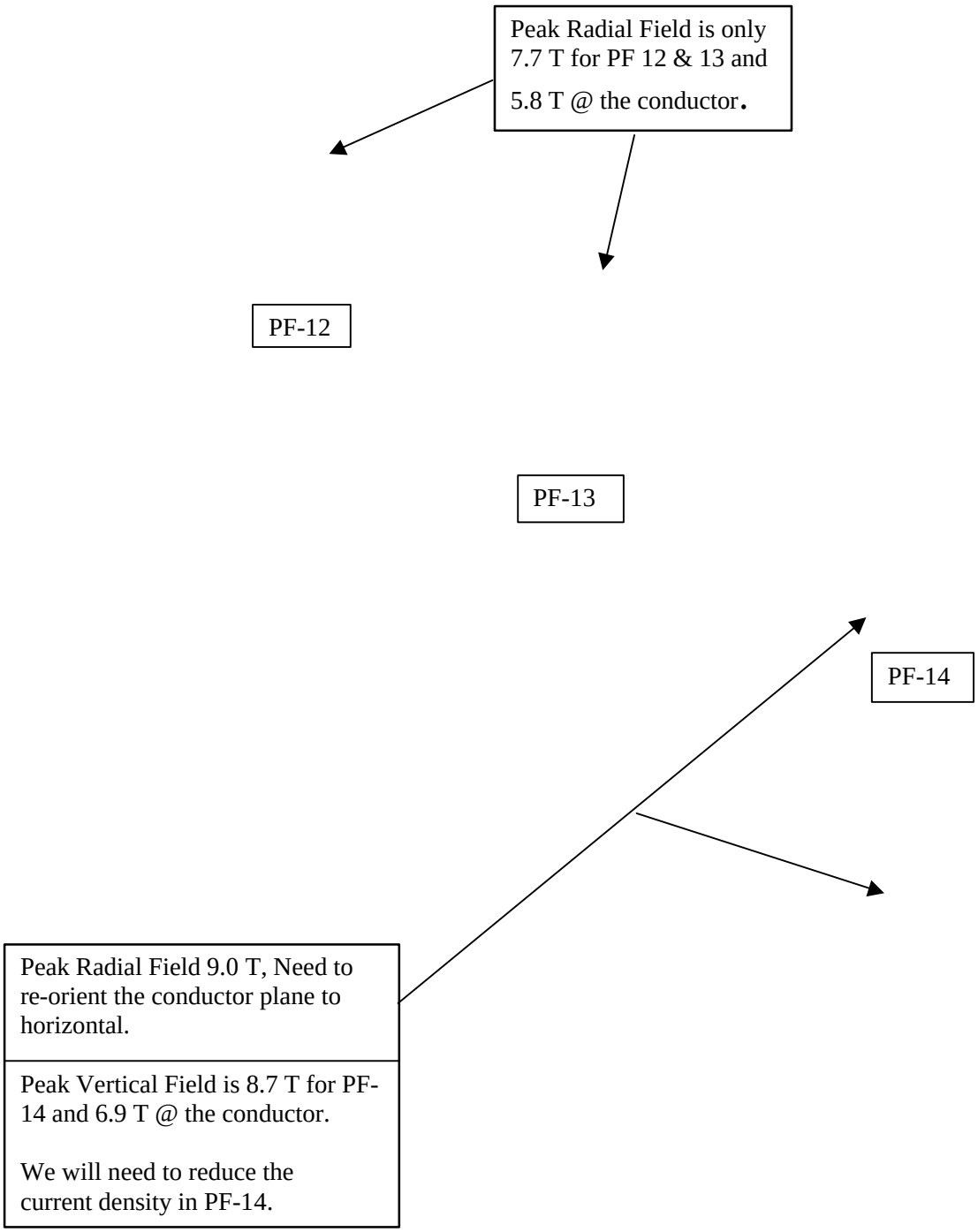

Figure 23. Radial Field Contours At the Outer PF Coils

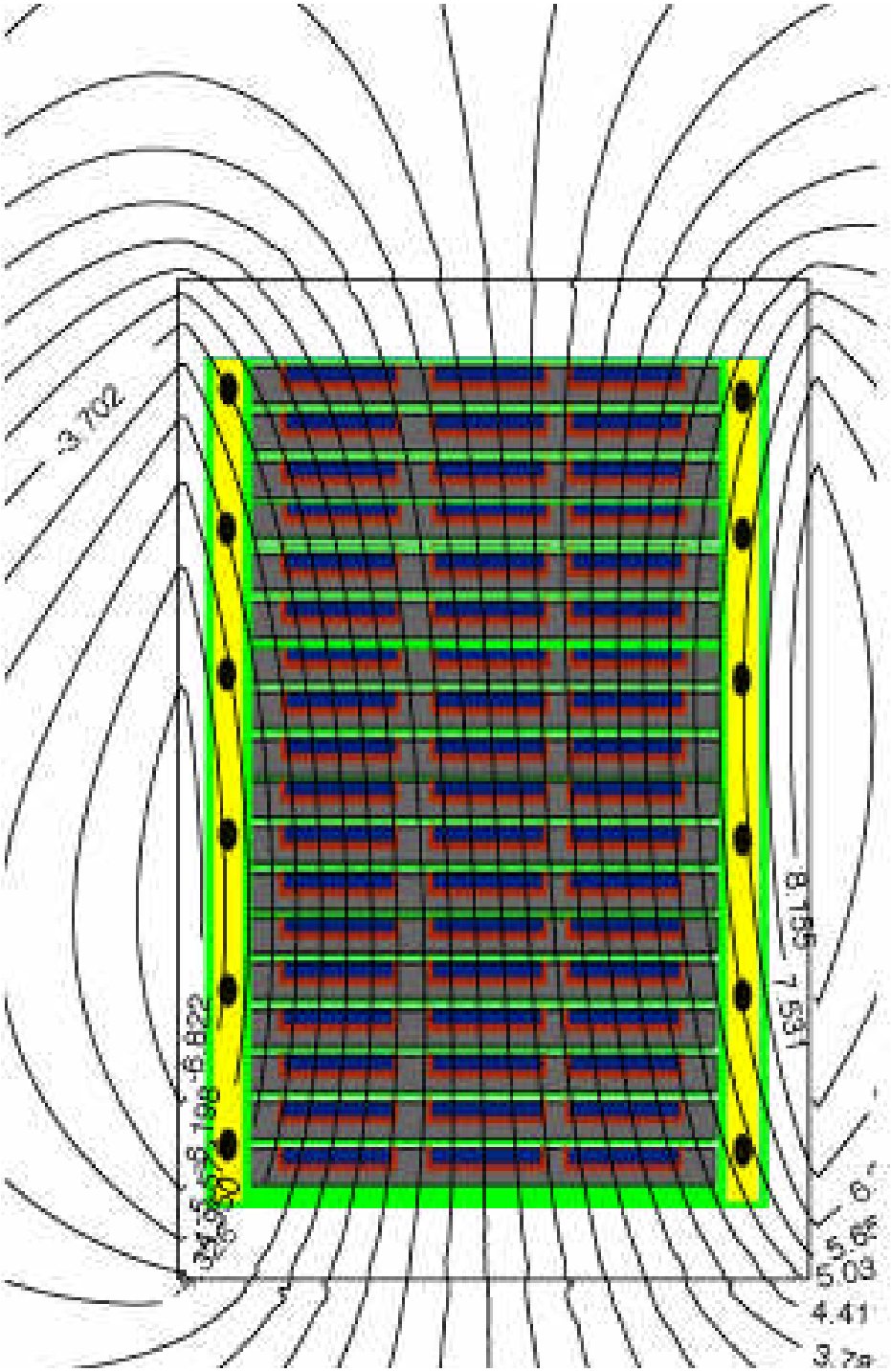

Figure 24. PF-14 Horizontal Conductors & 30kA/sq.mm – Vertical Field Contours

VII COIL COSTING:

In this section, the costing models of the TF and PF coils are described. A modification of the procedure for costing of the TF coils proposed during the previous studies was used. Although it is clear that a costing using cost per unit weight is very simplified, it was used for consistency with those previous studies.

Design studies using LTS materials use costing algorithms that result in costs that are substantially smaller than present day costs[10]. The reason for this, is use of conservative performance for the superconductor. With innovations in low temperature superconductors, (improved performance, copper laced, thin strands), and with improved manufacturing methods (react and wind, with stainless steel shell-like structure as proposed in this study), it would be possible to decrease the cost of the conductor by a factor of 6 and a cost of manufacturing by a factor of 2. The overall decrease in the cost of the coils as compared with present day costs would be about a factor of 4.

Large cost savings of the conductor are obtained by eliminating the stabilizer and quench protection, as well as in placing the cooling channels to the edge of the shells as described above.

The cost of the structural material ("ribbons" of 316 SS) has been assessed to be about $40/kg (cost of high-quality thin sheets of 316~SS at today's prices). Complex machining and cutting/welding of the structure is kept to a minimum.

The cost of the high temperature superconductor is difficult to estimate. Present day costs for commercially available low temperature superconductor (BSSCO 2212 or 2223), carries a cost premium over the low temperature superconductors of about a factor of 10. The cost penalty is in part due to the large amount of silver that is presently required in order to fabricate the superconductor. Although presently it is not possible to commercially acquire YBCO tapes, there are plans to start commercial manufacturing of HTS in 2003[10]. The costs are assumed using comparable techniques in the semiconductor industry, which imply $1000/kg for high quality films. Since the superconductor fraction is on the order of 1%, the cost of the winding would be about $50/kg.

Because of the advanced manufacturing process[12], few operations are needed to finish the coil after completing the winding (ground strap insulation followed by casing). The overall cost of the magnet could therefore be close to $50/kg.

It should be stressed that the cost of electricity is not very sensitive to the unit cost of the magnet, since the magnet size has been decreased due to improved plasma performance.

Table 4 compares the main characteristics of the magnets of ARIES-I, ARIES-RS, ARIES-ST and ARIES-AT. It can been seen that improved physics and engineering allowed the decrease in the stored energy of the TF magnet by about 25%, with substantially decreased peak toroidal field. However, the peak poloidal fields are comparable to those of ARIES-RS, but smaller than those of ARIES-ST (which required very large currents in the PF system).

VIII. CONCLUSIONS

This report has presented a conceptual design of the magnet systems for an advanced tokamak reactor. The intent was to anticpate and extrapolate the current state-of-the-art in high temperature superconductors and coil design, and apply them to an advanced reactor concept. Due to limited resources available no attempt has been made to optimize the coil/structure or other reactor subsystem interfaces beyond accomodating the requirements for radial maintenance of the blanket module. Regarding HTS, it does not offer significant SC advantages over low temperature superconductors for ARIES-AT, because of the decreased field requirements due to improved physics assumptions. The modest values of field and the stress limitations result in low overall current density in the magnet, achievable with the more conventional low temperature superconductors.

However, HTS does offer operational advantages over low temperature superconductors, including liquid nitrogen temperature operation, dry magnets, wide superconducting tapes (deposited directly on the structure) and reduced protection issues. These items result in substantial potential cost savings, due to ease of fabrication using advanced manufacturing techniques.

		ARIES-I	ARIES-RS	ARIES-ST	ARIES-AT
SC type		Nb3Sn/NbTi	Nb3Sn/NbTi	CU/SC PF	HTS
IcondTF	(kA)	100	51.2		2.6
IcondPF	(kA)		66.1 @ 9.3 T		2.3
			62 @ 13.8 T	47.4	
BmaxTF	(T)	21	16		11
BmaxPF	(T)		13.8	15.5	12
WmTF	(GJ)		51		38
JnoncuTF	(A/ mm2)	240	740		2500
JnoncuPF	(A/ mm2)		374	280 @ 15.5 T	2500
				651 @ 10.7 T	
JcuTF	(A/ mm2)		261		NA
JcuPF	(A/ mm2)		168	147.9	NA
VmaxTF	(kV)	20	20		NA
VmaxPF	(kV)		20		NA
sallowTF	(MPa)		800		
sallowTF	(MPa)		600		
sopTF	(MPa)	850	562		530
sopPF	(MPa)		561	571	530

Table III. Comparison between several previous ARIES designs and ARIES-AT

IV. REFERENCES:

1. [ARIES-RS] F. Najmabadi and the ARIES TEAM, Overview of the ARIES-RS reversed-shear tokamak power plant study, *Fusion Engineering and Design* **38** 3-27 (1997)

2. [ARIES-RS-magnet] Bromberg, L., P. Titus, J.H. Schultz, M. Sidorov, S. Pourrahimi and the ARIES Team, *ARIES RS Magnet Systems*, *Fusion Engineering and Design* **38** 159-188 (1997)

3. [Bromberg-01]L. Bromberg, M. Tekula, L. A. El-Guebaly, R. Miller, Options for the Use of High Temperature Superconductor in Tokamak Fusion Reactor Designs, Fusion Engineering and Design, to be published

4. [Maley] Maley, M.P. *et al.*, *Optimization of Transport critical current in HTS Conductors*, in *1996 Annual Peer Review Meeting, U.S. Department of Energy*, Washington D.C. (July 31, 1996).

5. [Bellis] Bellis RH, Iwasa Y. Quench propagation in high Tc superconductors, *Cryogenics*, **34** 129-44 (1994)

6. [CCAN] P.J.Gierszewski, A.S.Wan and T.F.Yang, *ccan and tcan - 1.5-d compressible-flow and time-dependent codes for conductor analysis*, MIT plasma fusion center report PFC/RR-83-1 (January 1983)

7. [Sauerzopf] F.M. Sauerzopf et al.: PRB 51 (1995) 6002-6012.

8. [Kupfer] H. Küpfer et al: Z. Phys. B 69 (1987) 167-171

9. [MSC/NASTRAN] The MacNeal-Schwendler Corp., LosAngles, Ca., MSC Software Inc.

10. [Schultz] Schultz, J.H., *Integration of High-Tc Superconductors into the Fusion Magnet Program*, MIT Plasma Science and Fusion Center Report PSFC/RR-99-5 (April 1999)

11. [ACS] See: http://www.amsuper.com/press/2000/Devens%20Final%20Release.pdf

12. [Waganer] Waganer, L.M. *Ultra-Low Cost Coil Fabrication Approach for ARIES-ST*, paper submitted to *Fusion Engineering and Design*, Jan 1999